



HAL
open science

The challenge of solar powered combined cycles e Providing dispatchability and increasing efficiency by integrating the open volumetric air receiver technology

Fritz Zaversky, Iñigo Les, Patxi Sorbet, Marcelino Sánchez, Benoît Valentin,
Jean-Florian Brau, Frédéric Siros

► To cite this version:

Fritz Zaversky, Iñigo Les, Patxi Sorbet, Marcelino Sánchez, Benoît Valentin, et al.. The challenge of solar powered combined cycles e Providing dispatchability and increasing efficiency by integrating the open volumetric air receiver technology. *Energy*, 2019, 194, pp.116796. 10.1016/j.energy.2019.116796 . hal-03366487

HAL Id: hal-03366487

<https://edf.hal.science/hal-03366487>

Submitted on 5 Oct 2021

HAL is a multi-disciplinary open access archive for the deposit and dissemination of scientific research documents, whether they are published or not. The documents may come from teaching and research institutions in France or abroad, or from public or private research centers.

L'archive ouverte pluridisciplinaire **HAL**, est destinée au dépôt et à la diffusion de documents scientifiques de niveau recherche, publiés ou non, émanant des établissements d'enseignement et de recherche français ou étrangers, des laboratoires publics ou privés.



The challenge of solar powered combined cycles – Providing dispatchability and increasing efficiency by integrating the open volumetric air receiver technology

Fritz Zaversky^{a,*}, Iñigo Les^a, Patxi Sorbet^a, Marcelino Sánchez^a, Benoît Valentin^b, Jean-Florian Brau^b, Frédéric Siros^b

^a National Renewable Energy Center (CENER), Solar Thermal Energy Department, Address: c/ Ciudad de la Innovación 7, Sarriguren (Navarra), Spain

^b EDF – R&D, 6 quai Watier, 78400, Chatou, France

ARTICLE INFO

Article history:

Received 12 November 2018

Received in revised form

19 November 2019

Accepted 17 December 2019

Available online 23 December 2019

Keywords:

Solar combined cycle

Reheated gas turbine

Volumetric receiver

ABSTRACT

This work analyzes the performance potential of solar-only powered combined cycles, comparing the impact of two different solar receiver technologies (opaque-heat-exchanger-type vs. volumetric). Due to material and receiver performance constraints, as well as the absence of internal combustion, the gas turbine inlet temperature (TIT) is limited to considerably lower values than observed in current fossil-fired state-of-the-art combined cycle plants. Therefore, the analysis includes the evaluation of a reheated topping Brayton cycle, aiming for a higher mean temperature of the heat input, thereby allowing fair conversion efficiencies despite moderate TITs. An extensive parametric optimization analysis compares different solar combined cycle configurations and benchmarks them against conventional CSP single-cycle plants. High thermal losses in the receiver tend to offset the gain allowed by the power cycle. The innovative coupling of an open volumetric air receiver with a regenerative heat exchange system that works in alternating operating modes (non-pressurized heating period, pressurized cooling period) could be a promising solution to efficiently drive a solar powered combined cycle. Furthermore, the optimum solar combined cycle performance for typical mean concentration ratios ($C \approx 500$) is fully compatible with high temperature TES, providing the promising possibility of fully dispatchable operation at highest thermal-to-electric conversion efficiency.

© 2019 The Authors. Published by Elsevier Ltd. This is an open access article under the CC BY license (<http://creativecommons.org/licenses/by/4.0/>).

1. Introduction

This work focuses on concentrated solar power (CSP), in particular on the central receiver technology [1] applying the combined cycle (topping GT plus bottoming steam Rankine) as thermodynamic power cycle.

The combined cycle technology [2] is well known from conventional fossil-fired power generation and reaches cycle efficiencies exceeding 60% on a lower heating value basis [3]. However, these best of class efficiencies are obtained with latest fossil-fired gas turbine (GT) technology, achieving turbine inlet temperatures (TITs) of up to ≈ 1500 °C. It is clear that such high TITs can only be achieved with (i) internal combustion, and (ii) turbine blade

cooling and single crystal super-alloy turbine blades, furthermore coated with low conductivity ceramics. For the application of solar combined cycles, the concept of externally-heated gas turbines [4] has to be exploited, which limits the maximum achievable TIT to considerably lower values (≈ 900 – 1000 °C).

Probably the first work that mentioned a solar driven combined cycle was that of Becker et al. [5]. The gas-cooled receiver's outlet temperature (maximum cycle temperature) was assumed at 800 °C, being roughly the upper feasibility limit for a metal tube receiver, resulting in a combined cycle efficiency (thermal-to-electric) of 39.1% [5].

Fraidenraich et al. [6] modeled the overall system performance of a solar-driven combined cycle plant and showed that there exists an optimum operating temperature for the solar receiver, which is in the range ≈ 927 – 1027 °C, depending on the number of bottoming Rankine cycle pressure levels. The optimum receiver operating temperature is fundamentally due to the dramatically increasing radiative heat losses at elevated temperatures that offset

* Corresponding author.

E-mail addresses: fzaversky@cener.com, fritz.zaversky@alumni.tugraz.at (F. Zaversky).

Nomenclature	
A_a	total aperture area (heliostat area times number of heliostats) (m^2)
A_r	receiver aperture area (m^2)
BC	Brayton cycle (externally heated open Brayton cycle)
C_{hyp}	hypothetical power tower concentration ratio: $\frac{A_a}{A_r}$ (–)
C_{flux}	effective solar flux concentration ratio: $\frac{I}{DNI}$ (–)
CPC	compound parabolic concentrator
CSP	concentrated solar power
DNI	direct normal irradiance (W/m^2)
GT	gas turbine
HEX	heat exchanger
HP	high pressure (HRSG)
HRSG	heat recovery steam generator
HTF	heat transfer fluid
h	receiver convective heat transfer coefficient ($W/(m^2K)$)
$h_{air\ in}$	specific enthalpy of air at HRSG inlet (J/kg)
$h_{air\ out}$	specific enthalpy of air at HRSG outlet (J/kg)
I	mean solar flux density (W/m^2)
IP	intermediate pressure (HRSG)
K	reheat ratio (–)
LP	low pressure (HRSG)
\dot{m}_{air}	HRSG air mass flow (kg/s)
P_{con}	receiver convective heat loss (W)
P_{HTF}	useful thermal power gained by heat transfer fluid (W)
P_{loss}	receiver heat loss (W)
P_{net}	net electric power (W)
P_{rad}	receiver radiative heat loss (W)
P_S	incident solar power at receiver (W)
P_{SF}	total power theoretically available for the solar field (W)
p_{ti}	turbine inlet pressure (Pa)
p_{to}	turbine outlet pressure (Pa)
PR	pressure ratio (–)
Solar efficiency	Solar-to-electric efficiency
T_a	ambient temperature (K)
TES	thermal energy storage
TET	turbine exit temperature
TIT	turbine inlet temperature
T_r	receiver temperature (K)
α	receiver solar absorptance (–)
ϵ	thermal emittance of receiver (–)
η_{cycle}	power cycle net efficiency (–)
$\eta_{c,i}$	isentropic compressor efficiency (–)
$\eta_{c,m}$	mechanical compressor efficiency (–)
η_g	generator electric efficiency (–)
η_f	solar field efficiency (–)
η_r	receiver efficiency (–)
$\eta_{t,i}$	isentropic turbine efficiency (–)
$\eta_{t,m}$	mechanical turbine efficiency (–)
σ	Stefan-Boltzmann constant ($W/(m^2 K^4)$)

the increase in power cycle performance. They estimated net solar power plant efficiencies (solar-to-electric) in the 23–25% range.

Kribus [7] studied an innovative beam-down plant configuration with CPC secondary concentrators before the pressurized air receiver (DIAPR [8]), able to deliver hot gas at a pressure of 10–30 bar and temperatures of up to 1300 °C to the topping gas turbine cycle. In combined cycle configuration, the obtained annual plant efficiency (solar-to-electric) was 21.3%, with a gross power conversion efficiency (thermal-to-electric) of 47%.

Puppe et al. [9] presented a detailed analysis of solar-hybrid combined cycle configurations, considering a parallel arrangement of solar receiver, high-temperature thermal energy storage (TES) and a fossil-fired combustion chamber. The nominal receiver outlet temperature was 950 °C; the nominal turbine inlet temperature after fossil combustion was 970 °C. They considered a pressurized solar receiver, a mixture of tubular cavity (low temperature) and pressurized volumetric receiver (high-temperature). Due to the parallel arrangement of receiver and TES, also the TES system (of regenerator type) needed to be pressurized. A power block net efficiency of 42.7%, and an annual solar-to-electric plant efficiency of about 22% was reported. A conceptually very similar approach was investigated by Grange et al. [10], differing in the receiver design approach (applying a metallic surface absorber located at the back of a cavity).

Poživil & Steinfeld [11] performed an optimization study of a solar-driven combined cycle power plant. They considered an innovative opaque-heat-exchanger-type pressurized air receiver consisting of a cylindrical cavity made of sintered α -silicon carbide (SiC) surrounded by a concentric annular reticulated porous ceramic (RPC) foam (also made from SiC), which exchanges heat with the pressurized air stream. A CPC secondary concentrator is attached to the windowless aperture to increase concentration ratio. For the specific parametric settings, they obtained an

optimum receiver operating temperature (gas turbine inlet) of 1200 °C.

Siros & Fernández-Campos [12] investigated the possible layouts of a low-TIT combined cycle gas turbine for the specific application of solar-driven combined cycles. In order to achieve reasonable efficiencies, alternative GT architectures (single reheat, or double reheat) must be applied to improve GT performance, and thus pushing the resulting combined cycle efficiency to just above 50% [12]. They concluded that (i) a reheated gas turbine must always be used whatever the TIT envisioned, (ii) at very low TIT (800 °C) a double reheat is interesting, and (iii), the intercooling of the compression is never of advantage. There is no major technological hurdle to build an uncooled, low-TIT and reheated gas turbine, other than designing and manufacturing the last heat exchanger train at reasonable cost [12] (bulky design due to relatively low air pressure).

It is clear that the solar receiver unit is the key component of a solar powered combined cycle plant, since it is of utmost importance to achieve very good solar receiver efficiencies at highest operating temperatures (≈ 1000 °C). So far, pressurized air receivers have been the design principle for solar-powered gas turbines, since the solar receiver has to provide heat to a pressurized air stream coming from the gas turbine's compressor. Several previous research projects have already endeavored to design such a demanding component, which has to operate under very high solar flux (≈ 0.5 – 1 MW/m²), at high temperatures (>900 °C), and in addition at pressures over 6 bar (depending on Brayton cycle configuration, as shown later on). The first developments started in the 1980's with metallic and ceramic tubular designs [13]. This approach showed however durability issues and also low efficiencies because of the low heat transfer coefficient of air. Therefore, pressurized volumetric receivers [14] appeared to be a promising alternative as they increased the heat transfer area.

However, durability issues and size limitations of the needed quartz glass window have hindered their commercial application so far. For this reason, the idea of pressurized tubular or opaque-heat-exchanger-type receivers was revisited by several research groups. For example, Grange et al. [10] investigated a modular metallic absorber located at the back of a cavity. The maximum air outlet temperature was reported to be 750 °C. Korzynietz et al. [15] developed a pre-commercial scale metallic tubular cavity receiver achieving thermal efficiencies between 71.3% and 78.1% at the maximum air outlet temperature of 800 °C.

According to the available literature, solar powered combined cycles have already been subject of several investigations and show promising solar-to-electric conversion efficiencies. However, although dispatchability is the key advantage of CSP (due to cost-effective thermal energy storage - TES), and its only argument to justify higher costs than PV or wind energy, only a few works have covered so far the integration of high-temperature TES upstream the solar combined cycle.

The aim of this work is therefore to present an innovative plant layout that not only avoids the design challenges related to pressurized receivers, but also allows the integration of an atmospheric air based high-temperature TES system upstream the combined cycle. In particular, this work proposes the application of the open volumetric air receiver technology [14], which has already been demonstrated successfully at pre-commercial scale [16], in combination with a regenerative system working in alternating modes (atmospheric heating, pressurized cooling – see Fig. 1) in order to drive a solar-only powered combined cycle. This approach decouples the high temperature and the high heat flux part (solar receiver) from the high pressure part (compressed air stream of the Brayton cycle) via an air-air regenerative heat exchanger.

Clearly, the options for the required high-temperature (≥ 1000 °C) TES are limited. When using open volumetric air receivers, the well proven and relatively cheap regenerator-type heat storage known from so-called Cowper Stoves [18] can be used. This type of regenerative heat storage has already been demonstrated successfully at pilot plants [19] for the application of CSP. The big advantages of this technology are (i) a simple design with very low technological risk, and (ii) low costs (≈ 17 €/kWh_{th} [20]). Unlike the approaches presented in Refs. [9,10], which require a pressurized regenerative TES, the proposed innovative concept, which applies an atmospheric volumetric receiver, allows the direct integration of an atmospheric regenerator-type TES (see Fig. 2), which has clear engineering and cost advantages.

It must be emphasized that the temperature level of the “cold” return air stream, leaving the air/air heat exchange system, is a

function of compressor outlet temperature (i.e. compressor pressure ratio and ambient temperature) and the exit temperature of the first turbine stage, in the case of reheat. The resulting air-return temperature level is too high for efficient blower operation and the recirculation to the high-temperature TES or the receiver is thus not feasible. A low-temperature air/rock thermozone TES is thus proposed in order to reuse the return air heat in regenerative manner. In order to keep air transport parasitic power consumption acceptable, the operating temperature of the blower should be kept at ambient temperature level.

The proposed plant concept implies the challenge of designing an economical HTF-to-working-fluid heat exchanger for “firing” the topping Brayton cycle externally. In order to provide a good heat exchange effectiveness, this work proposes a regenerative heat exchange system working under atmospheric charging, and pressurized discharging conditions [17] (see Figs. 1 and 2). Clearly, the vessel size of this regenerative heat exchange system is limited due to the pressurization process, which requires several two-vessel subunits (as shown in Fig. 1) in parallel depending on the power rating. The second reason for several two-vessel subunits in parallel is the requirement for continuous thermal power transfer (while one system is pressurized/depressurized, the parallel systems need to take over).

The aim of this work is to show the performance potential of this innovative plant layout (Fig. 2) and benchmark it against conventional CSP technology, stating achievable conversion efficiencies of incident solar direct normal irradiance into electric power, i.e. peak solar-to-electric plant efficiencies. In particular, three points should be clearly shown: (i) the impact of reheat in the topping Brayton cycle on solar efficiency, (ii) the impact of ideal volumetric solar receiver performance (“volumetric effect”), and (iii) whether the optimum receiver operating temperature of the purely solar-powered combined cycle is compatible with available high-temperature TES technology, in order to provide dispatchability of the solar plant.

State-of-the-art CSP plants apply subcritical Rankine steam cycles, having live steam parameters either around 371 °C and 100 bar (parabolic trough plants with thermal oil as HTF), or 545 °C and 125 bar (central receiver plants using molten salt as HTF). Therefore, real-world state-of-the-art power cycle conversion efficiencies (thermal-to-electric) approximately range between 30 and 40%, critically depending on prevailing ambient temperature (typically very high at CSP locations) as well as the applied condenser technology (dry or wet cooling). For this reason, the application of the combined cycle (topping GT plus bottoming Rankine steam cycle) seems to be a promising development step in order to boost the

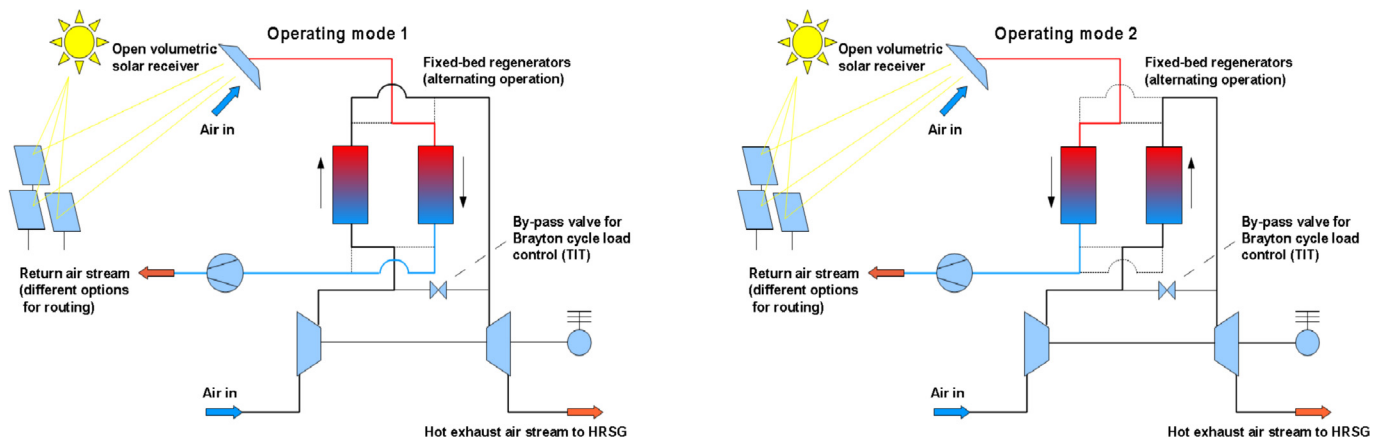


Fig. 1. Innovative coupling of open volumetric air receiver and Brayton cycle (CAPTURE concept [17]).

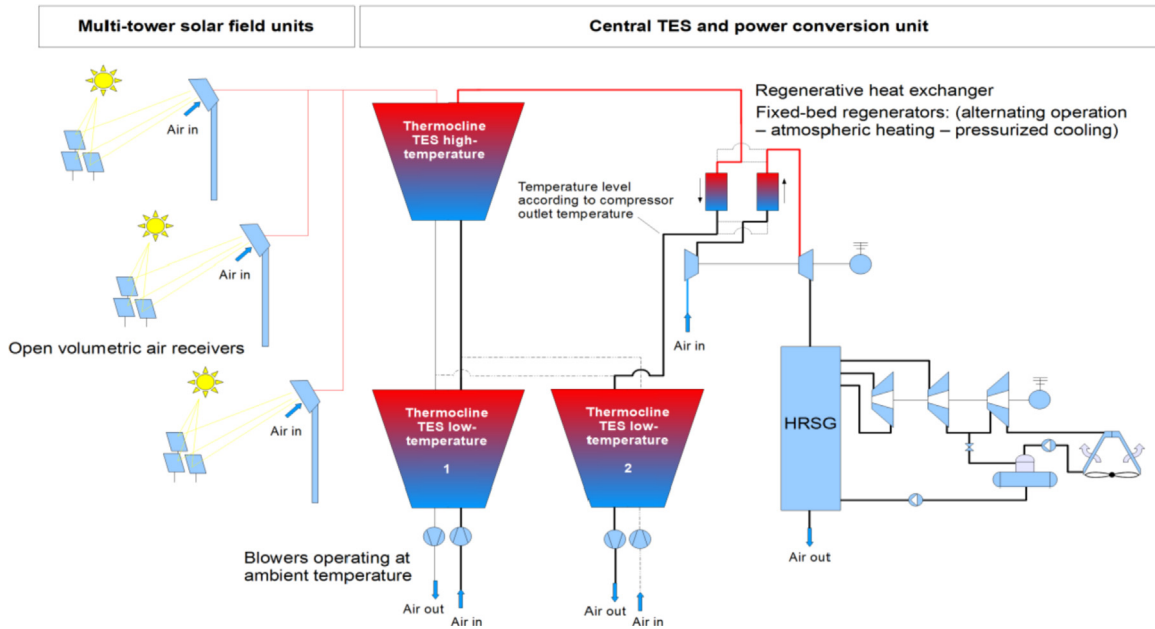


Fig. 2. Solar powered combined cycle scheme with open volumetric air receiver and high-temperature TES (without reheat in the Brayton cycle) – The low-temperature TES enables regenerative use of return air heat.

thermal-to-electric conversion efficiency towards the 50% target. However, so far, the need for high receiver operating temperature (≈ 1000 °C) and the demand for TES (allowing dispatchable operation of the combined cycle) have been imposing substantial design challenges with no clear solution. This work proposes a new approach (Fig. 2), combining both (i) reliable receiver operation at good conversion efficiency, and (ii) the possibility of cost-effective integration of TES upstream the combined cycle, allowing dispatchable operation at highest solar-to-electric conversion efficiency.

2. The motivation for a reheated Brayton cycle and its application in the context of combined cycle power generation

Reheated gas turbines have already been treated in previous works. The main motivations are (i) to keep the average temperature of heat supply high and (ii) to introduce an additional flexibility regarding turbine exit temperature, TET (the heat recovery steam generator inlet temperature), despite high compressor pressure ratios [21]. In particular, the expansion ratio of the second turbine stage can be specifically designed, so that the resulting TET optimizes the overall combined cycle performance.

As proposed by Siros & Fernández-Campos [12], the reheat pressure level will be defined by a dimensionless parameter K (reheat ratio), which determines the ratio of pressure ratios of both turbine stages:

$$K = \frac{\text{pressure ratio of first stage}}{\text{pressure ratio of second stage}} = \frac{\frac{p_{t1i}}{p_{t1o}}}{\frac{p_{t2i}}{p_{t2o}}} = \frac{p_{t1i} \cdot p_{t2o}}{p_{t1o} \cdot p_{t2i}} \quad (1)$$

Assuming no pressure drop in the HTF-to-working-fluid heat exchanger ($p_{t1o} = p_{t2i}$), simplifies the above equation to:

$$K = \frac{p_{t1i} \cdot p_{t2o}}{p_{t1o}^2} \quad (2)$$

Here, three considerations must be kept in mind:

- (i) The reheat ratio K is a key parameter concerning Brayton cycle performance (on its own) as well as combined cycle performance, nevertheless, it has different optimums for the single cycle and the combined cycle. The lower the pressure ratio of the second turbine stage is, the higher the turbine exit temperature (TET), i.e. HRSG inlet temperature, and thus the higher the efficiency of the bottoming Rankine cycle, but the lower the Brayton cycle performance. As later on shown, solar combined cycle performance optimizes in the interval $0.5 < K < 1.25$. The optimum value of K depends on concentration ratio, the corresponding optimum TIT, and HRSG efficiency. Note that Brayton cycle performance in single-cycle configuration (i.e. without bottoming Rankine cycle) optimizes for values of K lower than in the case of combined cycle (see Ref. [22]).
- (ii) Furthermore, the lower the pressure ratio of the second turbine stage is, the lower is the reheat pressure level and thus the bulkier and more expensive the second HTF-to-working-fluid heat exchanger will be. And the pressure drop would increase. Thus, there is clearly a lower practical limit for the second turbine stage's pressure ratio.
- (iii) Having higher pressure ratios in the first turbine stage means lower TET at the first stage and thus corresponds to a lower return temperature of the TES medium (thus higher ΔT for the TES, see Fig. 5). Thus, higher pressure ratios in the first turbine stage are not only preferred in terms of Rankine cycle performance (see point (i)), but also regarding integration with thermal energy storage (second heat exchanger train).

For the optimization of a solar-only-powered combined cycle, the following performance models are required:

- (i) The model of the solar-to-thermal energy conversion process, i.e. the heliostat field and the solar receiver performance.
- (ii) The model of the power cycle, i.e. the thermal-to-electric energy conversion process, which can be split into Brayton and Rankine cycle performance models.

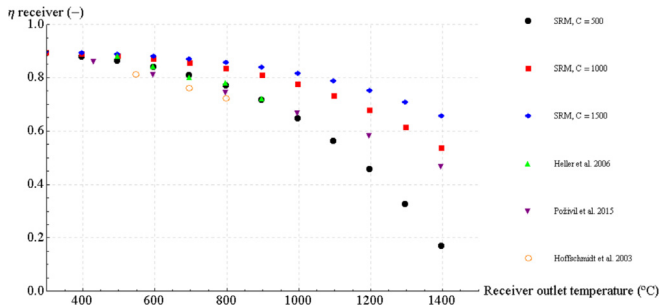


Fig. 3. Receiver performance according to simplified receiver model (SRM) and data in Refs. [27–29].

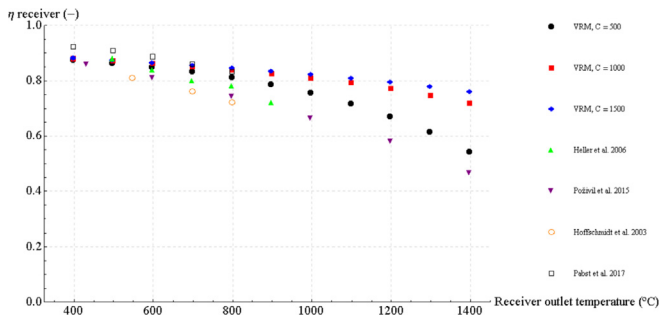


Fig. 4. Receiver performance according to volumetric receiver model (VRM) [30] and data in Refs. [27–29,32].

The resulting solar-to-electric efficiency, or simply solar efficiency, is the product of solar-to-thermal efficiency and thermal-to-electric efficiency.

3. Solar receiver and heliostat field performance – solar-to-thermal energy conversion

The solar receiver performance is principally governed by two factors, (i) the heat loss by thermal radiation, and (ii) the incident mean solar flux density. The first factor, the thermal radiation loss is a function of the absorber’s emittance ϵ , the receiver area A_r , as well

as the receiver surface temperature T_r . The second factor, the incident mean solar flux density is a function of the plant’s concentration ratio C . Concentration ratios range from 200 to 1000 suns for conventional power tower configurations without secondary concentrator [7,23]. Higher concentration ratios, i.e. higher mean solar flux densities, allow higher receiver efficiencies as the same thermal power can be achieved with smaller receiver aperture areas, thus less thermal losses (at the same operating temperature) and as a result higher thermal receiver efficiencies.

Here it is important to note that it has to be distinguished between the hypothetical power tower concentration ratio C_{hyp} , which is defined by the ratio of total aperture area (heliostat area times number of heliostats) to receiver aperture area (A_r), and the effective solar flux concentration ratio C_{flux} , defined by the ratio of incident mean solar flux density at the receiver I (W/m^2) to direct normal irradiance (DNI).

$$C_{hyp} = \frac{A_a}{A_r} \tag{3}$$

$$C_{flux} = \frac{I}{DNI} \tag{4}$$

Whereas C_{hyp} is a theoretical number, which will never be achieved in real life conditions due to optical losses, C_{flux} is a realistic characteristic number of a power tower plant, taking into account the entire optical losses from first reflection of sunlight at the heliostats to interception at the receiver aperture area. Thus, C_{flux} is always smaller than C_{hyp} ($C_{flux} < C_{hyp}$), and the ratio C_{flux} to C_{hyp} is defined by the optical efficiency η_f of the heliostat field, as shown with Eq. (5) and Eq. (6).

$$I = \frac{A_a \cdot DNI \cdot \eta_f}{A_r} = C_{hyp} \cdot DNI \cdot \eta_f \tag{5}$$

$$C_{flux} = \frac{I}{DNI} = C_{hyp} \cdot \eta_f \tag{6}$$

The further analysis will be based only on the effective solar flux concentration ratio C_{flux} , or simply C .

Next, the receiver’s thermal efficiency can be very well approximated by the following simple equation (Eq. (7)) [24,25]. Its

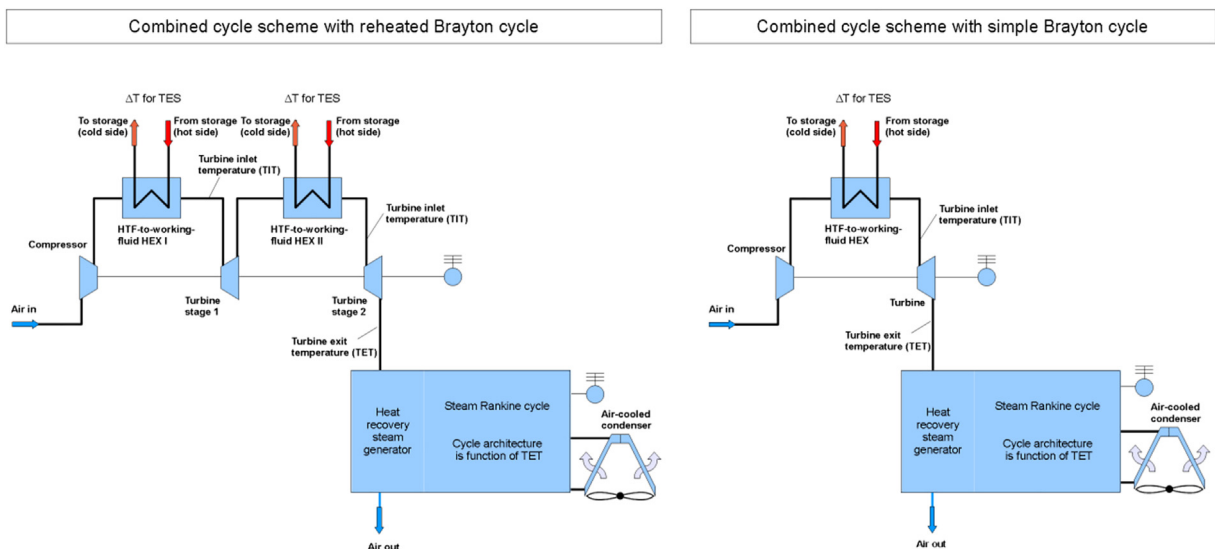


Fig. 5. Combined cycle scheme with reheated topping cycle and generalized TES interface (left); Equivalent scheme without reheat in the Brayton cycle (right).

derivation is given in the Appendix.

$$\eta_r = \alpha - \frac{\epsilon \cdot \sigma \cdot (T_r^4 - T_a^4) + h \cdot (T_r - T_a)}{C_{flux} \cdot DNI} \quad (7)$$

The solar-to-thermal efficiency of a central receiver plant can then be obtained by multiplying the solar field efficiency η_f by the receiver efficiency η_r (also see Appendix):

$$\eta_{solar-to-thermal} = \eta_f \cdot \eta_r \quad (8)$$

The solar field efficiency typically takes into account the mirror reflectivity, cosine loss, blocking and shading, spillage (interception) as well as atmospheric attenuation. Peak solar field efficiencies range from rather low values (≈ 0.55) for big surrounding heliostat fields with slant ranges of up to 1.8 km, to values of ≈ 0.8 for compact multi-tower heliostat fields (north fields in northern hemisphere) with maximum slant ranges at around 800 m (depending on solar field optimization algorithm). Generally it can be said, the smaller the field is, the higher is its efficiency.

For example, compact heliostat fields with an aperture area of about 80,000 m² (north fields) and designed for 55.27 MW receiver inlet power, reach annual efficiencies of about 71%, with peak values of just over 80% [26].

In order to offer the full performance potential for the heliostat field, in this work only compact multi-tower heliostat fields with a peak optical efficiency of 0.8 are taken into account, which is very likely to be the field design of next generation power tower plants, as compact heliostat fields provide significantly better efficiencies and better solar flux control. The aim of the present study is therefore to show the potential of a solar powered combined cycle assuming a multi-tower assigned-aiming heliostat field configuration, providing a peak optical efficiency of 0.8. The final heliostat field is thus an array of several identical subfields (the number depends on the needed nominal solar power). A reasonable size would be up to 6 fields (330 MW total nominal solar power). When increasing the number of towers, the HTF transport tends to become an issue.

The next section will justify the assumed receiver modeling methodology (Eq. (7)), and will furthermore show the improvement potential of advanced volumetric receivers.

3.1. Receiver efficiency plots – non-volumetric vs. volumetric

The quite simple receiver performance model, as given in Eq. (7), will be compared to receiver performance documented in public literature. In particular, it will be compared to data given in the work of Hoffschmidt et al. [27] (HiTRec II open volumetric receiver), Heller et al. [28] (SOLGATE pressurized air receiver), and Poživil et al. [29] (opaque-cavity-type pressurized air receiver). Fig. 3 shows the comparison of the results according to Eq. (7) (evaluated for 3 concentration ratios and one DNI level: $C = 500$, $C = 1000$, $C = 1500$; $DNI = 1000 \text{ W/m}^2$; $\alpha = 0.9$, $\epsilon = 0.8$, $h = 8 \text{ Wm}^{-2}\text{K}^{-1}$) with the data given in Refs. [27–29].

As can be seen, the theoretical receiver performance (Eq. (7)) for a concentration ratio of $C = 500$ (black dots) correlates very well with the data published by Heller et al. [28] (green triangles). Also the data published by Poživil et al. [29] (purple triangles inverted) correlates well below receiver outlet temperatures of about 1000 °C. Above that temperature threshold, the cavity effect (which lowers the effective heat loss area for thermal radiation) seems to become dominant, resulting in significant better performance at higher receiver operating temperatures. The data published by Hoffschmidt et al. [27] (orange circles), gives slightly lower efficiencies as estimated by Eq. (7).

The red cubes in Fig. 3 show the performance at concentration ratio $C = 1000$, the blue rhombi show the performance at concentration ratio $C = 1500$. It can be seen that higher concentration can significantly improve receiver performance at very high temperatures ($> 1000 \text{ °C}$), as well as at intermediate receiver operating temperatures (600–1000 °C). Nevertheless, it has to be kept in mind that this is a purely theoretical consideration. Real life concentration values for central receiver heliostat fields are not homogeneously distributed, in fact, local values above 1500 suns may be achievable with current heliostat field layouts. In practice, 500 suns is a good approximation for mean concentration, with values at about 1000 for the central part of the receiver. A mean solar flux at the receiver aperture of $\approx 1 \text{ MW/m}^2$ is the typical practical limit, due to real life concentration limits.

For the first optimization runs of the solar-driven combined cycle plant, Eq. (7) will be used for modeling the solar receiver performance. As a next step, the simple receiver model (Eq. (7)) will be replaced by an efficiency matrix (see Table 1) obtained by multiple parametric simulation runs of a 1-D ceramic foam volumetric absorber model [30]. The model has been successfully benchmarked against other codes [31], and against experimental data at operating temperatures of up to 600 °C [30]. Although the code has not been validated so far experimentally at relevant receiver operating temperatures of a solar-driven combined cycle plant ($\approx 1000 \text{ °C}$), and no experimental validation of the volumetric effect can be given at the moment, it has to be emphasized that the efficiency level for receiver outlet temperatures of 700 °C and 800 °C as indicated in Fig. 4 has been confirmed recently experimentally by Pabst et al. [32] (black hollow cubes in Fig. 4). Pabst et al. [32] presented experimental results with highly porous metallic volumetric absorbers, heating air up to 800 °C. The maximum long-term operating temperature limit of the applied alloy was 950 °C.

As can be seen in Fig. 4, the volumetric receiver promises better performance at high operating temperature with respect to non-volumetric opaque-heat-exchanger-type receivers. This is the crucial factor when considering overall solar combined cycle performance, as later on shown in Section 5.

4. The power cycle modeling – thermal-to-electric energy conversion

Fig. 5 shows the scheme of the combined cycle configurations

Table 1
Ceramic foam volumetric absorber performance matrix (absorber depth = 30 mm, cell diameter = 1.122 mm, strut thickness = 0.195 mm, porosity = 0.87, $\alpha = 0.9$, $\epsilon = 0.8$, $DNI = 1000 \text{ W/m}^2$).

Concentration ratio C (–)	Receiver air outlet temperature (°C)										
	400	500	600	700	800	900	1000	1100	1200	1300	1400
	η_r (–)	η_r (–)	η_r (–)	η_r (–)	η_r (–)	η_r (–)	η_r (–)	η_r (–)	η_r (–)	η_r (–)	η_r (–)
500	0.874	0.862	0.849	0.832	0.811	0.785	0.754	0.716	0.670	0.612	0.542
1000	0.880	0.872	0.862	0.852	0.840	0.826	0.810	0.792	0.771	0.747	0.718

analyzed. On the left, with reheated Brayton cycle and generalized TES interface, on the right, the equivalent scheme with simple Brayton cycle. Note that the detailed tube bundle and steam drum configuration of the heat recovery steam generator (HRSG), as well as Rankine cycle architecture is not shown for the sake of simplicity. A variety of bottoming Rankine cycle configurations are treated as function of HRSG gas inlet temperature (TET).

Whilst the modeling of the Brayton cycle is straight forward and quickly implemented according to the isentropic relationships for air as ideal gas, the modeling of the bottoming Rankine cycle is more complex, since (i) reliable thermodynamic properties of water and steam are required [33], (ii) the heat recovery steam generator needs to be optimized according to gas inlet temperature, choosing appropriate steam pressure levels and live steam temperatures, and (iii), the condensing pressure needs to be adapted to take variable ambient temperature into account (for annual simulation runs that are needed for calculating the plant's annual mean conversion efficiency – Table 6). Due to this rather complex problem, a performance table of the Rankine cycle has been generated with the help of a separate simulation tool (GT PRO) [34].

4.1. Modeling of the externally-heated Brayton cycle

The modeling of an un-cooled gas turbine is straight forward. The simple isentropic relationships for air as ideal gas can be applied and can be obtained from any thermodynamics textbook. Fluid properties (dry air) have been implemented according to McBride et al. [35]. The applied turbomachinery parameters are given in Table 2.

4.2. Modeling of the bottoming Rankine cycle

In order to select the best possible TET, several air-cooled steam Rankine cycles were designed for TET ranging from 400 to 1100 °C. The Rankine cycle simulations were performed using a state-of-the-art power cycle simulation software [34], which allows the design and steady-state simulation of HRSGs, taking into account industrial standards.

The Heat Recovery Steam Generator (HRSG) is aimed at recovering as much heat as possible from the Brayton cycle exhaust (which is best performed by using low-pressure steam), while enabling a good Rankine cycle conversion efficiency (best achieved at high steam pressures). For every TET, a case study was performed in GT PRO, letting the HP, IP (when relevant) and marginally LP pressures vary in order to maximize the power output of the Rankine cycle, considering a hot air flowrate of 240 kg/s in the HRSG, which roughly corresponds to a 100–150 MWe plant. The steam parameters are chosen not to exceed 190 bars and 600 °C, in order to remain coherent with industrial standards.

In each case, simulations were run with ambient temperatures ranging from 0 to 40 °C, considering a temperature difference of 20 °C between the condensing temperature and the ambient. The isentropic efficiencies of all three turbine stages were estimated by GT PRO; they range from 84.4% to 89.4% across the HP stage, 89.3%–

92.2% across the IP stage and 84%–93.7% for the LP stage. The isentropic efficiency of HRSG feed pumps was set to 75%.

The architecture thus offering the best compromise between heat recovery and conversion efficiency (i.e. the maximum net electric power) changes with the TET: (i) from 400 to 600 °C, it has 3 levels of pressure, but no reheat, as it would be too detrimental to either the heat recovery or the turbine efficiency, (ii) at 700 °C and above a reheat becomes profitable, and (iii) above 900 °C the amount of heat to recover, and therefore the steam flowrate in the HRSG, become so great that there is no longer any pinch limitation at the evaporators. One HP level is then sufficient, the LP evaporator only feeding the deaerator (integral deaerator design [36] in this case).

The steam pressures in each architecture and cycle performance are detailed in Table 3. It should be noted that the superheater tubes are assumed to be sufficiently cooled by the steam flow in order to avoid excessive tube material temperature, despite very high HRSG air inlet temperatures.

$$\eta_{\text{cycle}} = \frac{P_{\text{net}}}{\dot{m}_{\text{air}} \cdot (h_{\text{air in}} - h_{\text{air out}})} \quad (9)$$

5. Performance of the solar combined cycle and benchmarking against single-cycle plants

The above presented performance models have been implemented into one complete solar thermal power plant model (in Modelica [37]) enabling a full parametric analysis and optimization of the solar-to-electric efficiency, employing the Modelica scripting feature in order to run the model automatically for a large number of cases (≈ 1500). The varied parameters are receiver outlet temperature, compressor pressure ratio, the reheat ratio K and the concentration ratio C of the solar system.

For the definition of the Brayton cycle outlet pressure, a HRSG gas pressure drop of 1.5 kPa is assumed. This is a typical upper range value according to Ganapathy [38], who gives a HRSG gas pressure drop range between ≈ 0.8 and 1.5 kPa [38].

It is assumed that the gas turbine inlet temperature is equal to the receiver outlet temperature. On the one hand, this is a quite realistic assumption for the case of pressurized air receivers (e.g. receivers according to Ref. [28] or Ref. [29]) and for the regenerative gas-gas heat exchanger approach considered in this work (see Figs. 1 and 2 – regenerative HEX scheme), as the effectiveness of direct contact heat exchangers is very high. Nevertheless, when applying a high-temperature thermocone TES upstream the combined cycle, the outlet temperature of the TES system will not be constant, i.e. will decrease during discharge operation. Also, thermal losses in the piping will reduce the TIT slightly. For this reason, the numbers given in the following are ideal conversion efficiencies under nominal conditions only. It is clear that the TES system's outlet temperature decrease needs to be taken into account in detailed annual performance calculations, which requires the modeling of the power cycle under part load conditions.

It must be emphasized, that the performance of the solar thermal power plant will be evaluated under two assumptions:

- (i) The solar receiver has “non-volumetric” behavior, and its behavior is assumed to be sufficiently well reproduced by the simple performance relationship according to Eq. (7). This case would be valid for volumetric air receivers with non-ideal behavior (i.e. the volumetric effect does not occur), opaque-heat-exchanger-type receivers or particle receivers without cavity effect.

Table 2
Turbomachinery parameters.

Parameter (Unit)	Value
Isentropic efficiency compressor $\eta_{c,i}$ (–)	0.85
Isentropic efficiency turbine stages $\eta_{t,i}$ (–)	0.9
Mechanical efficiency compressor $\eta_{c,m}$ (–)	0.97
Mechanical efficiency turbine stages $\eta_{t,m}$ (–)	0.97
Generator electric efficiency η_g (–)	0.97

Table 3
Rankine cycle performance table as function of HRSG air inlet temperature and ambient temperature (specific net power and net efficiency).

HRSG Air temperature inlet (°C)	400	500	600	700	800	900	1000	1100
Live steam temperature (°C)	380	480	580	600	600	600	600	600
Steam pressure level – HP/IP/LP or HP/LP (bar)	30/9/2.5	50/12/2.5	80/16/2.9	190/22/3 RH	190/22/3 RH	190/3 RH	190/3 RH	190/3 RH
Ambient temperature (°C)	Condensing pressure (bar)							
	Specific net power (kWe/(kg/s) of air) / Net efficiency η_{cycle} (%)							
40	0.19	68 / 22.8%	111 / 26.7%	163 / 30.5%	228 / 34.9%	281 / 36.2%	335 / 37.0%	386 / 37.3%
30	0.17	74 / 24.3%	119 / 28.1%	172 / 31.7%	240 / 36.2%	295 / 37.5%	350 / 38.3%	403 / 38.6%
20	0.1	80 / 25.8%	126 / 29.4%	180 / 32.9%	251 / 37.5%	308 / 38.7%	365 / 39.4%	419 / 39.7%
10	0.06	85 / 27.2%	133 / 30.7%	189 / 34.1%	261 / 38.7%	320 / 39.8%	379 / 40.6%	435 / 40.8%
0	0.04	90 / 28.5%	139 / 32.0%	197 / 35.1%	271 / 39.7%	333 / 41.1%	392 / 41.5%	446 / 41.8%

(ii) The solar receiver has “volumetric” behavior, i.e. the so-called volumetric effect occurs and its behavior can be estimated by interpolating Table 1

In the performed simulations, the pressure drop of the Brayton cycle’s HTF-to-working-fluid heat exchanger is kept at a reasonable value of 3% of compressor outlet pressure. Note that this value is taken for each heat exchanger train, i.e. 2 times for single reheat. Also the DNI level and the ambient temperature are kept constant (peak solar-to-electric efficiency evaluation). The DNI level is set to a typical maximum value observed at CSP locations (1000 W/m²), the ambient temperature is set to a moderate value of 25 °C, which should be realistic for operation after sunset (TES discharging).

The varied parameters (receiver temperature - TIT, pressure ratio, reheat ratio K and C) are all key parameters that have a substantial impact on the overall performance. In particular, the concentration ratio limits the maximum receiver operating temperature. Thus, the lowest concentration ratio will have the lowest optimum receiver operating temperature and thus the lowest TIT. Thus it makes sense to optimize the remaining three parameters (receiver temperature -TIT, pressure ratio and reheat ratio K) for each concentration ratio C separately. The fundamental point in the optimization process is that the reheat ratio K introduces the possibility to maintain a high overall pressure ratio (thus keeping BC efficiency high), while having a low expansion ratio at the second turbine stage, thus achieving a high TET, which improves the bottoming Rankine cycle efficiency. Nevertheless, there exists a practical upper limit for the reheat ratio K , as the lower pressure level at reheat, reduces the fluid density, and thus pressure drop and heat transfer constraints will necessitate a very bulky and probably too costly second heat exchanger train.

5.1. Performance of the solar combined cycle with non-volumetric receiver behavior

The analysis of the solar combined cycle’s overall efficiency is started with concentration ratio C equal to 500. In particular, the BC pressure ratio is optimized for 5 values of the reheat ratio K (1.5, 1.25, 1, 0.75 and 0.5) separately. Table 4 gives the respective values of TIT and pressure ratio (PR) that optimize the solar-to-electric conversion efficiency. Note that the results consider peak solar-to-electric conversion efficiency, assuming a solar field efficiency (η_f) of 0.8 (see Section 3).

Fig. 6 displays the solar-to-electric conversion efficiency as function of TIT and gas turbine pressure ratio for concentration ratio $C = 500$ and reheat ratio $K = 1.25$. The optimum conversion efficiency is obtained at a turbine inlet temperature (receiver outlet temperature) of ≈ 875 °C and a pressure ratio of about 7.

As can be seen in Table 4, the conversion efficiency for concentration ratio $C = 500$ optimizes when $K = 1.25$. However, the variation in efficiency for the analyzed values of K is below 1 percentage point. Thus, considering the size limitation of the second

Table 4
Optimum values of reheated BC TIT (receiver outlet temperature) and PR for given values of K .

C (-)	K (-)	optimum TIT (°C)	optimum PR (-)	$\eta_{\text{solar-to-electric}}$ (%)
500	1.5	850	6	27.1%
500	1.25	875	7	27.1%
500	1	900	8	26.9%
500	0.75	900	8	26.7%
500	0.5	900	12	26.2%
1000	1.5	1000	14	30.8%
1000	1.25	1000	14	31.0%
1000	1	1000	14	31.1%
1000	0.75	1050	14	31.0%
1000	0.5	1050	12	30.7%

heat exchanger train and the small differences in efficiency observed, a value of K in the range 1–1.25 is deemed to be reasonable. Here it must be noted that the impact of K depends on the Rankine cycle’s sensitivity to the HRSG’s inlet temperature. In particular, the more effort is made in heat recovery (steam pressure level optimization), the lower is the impact of K .

A similar relationship can be observed when analyzing the simulation results for concentration ratio $C = 1000$ (Fig. 7). However, the optimum value of K moves to a lower value ($K = 1$) as the increase in concentration ratio allows a higher receiver working temperature and thus a higher TIT, which improves the BC performance and thus its relative impact on combined cycle efficiency.

Fig. 8 shows the achieved combined cycle thermal-to-electric conversion efficiency as a function of the turbine inlet temperature and pressure ratio of the topping reheated Brayton cycle ($K = 1.25$).

For a turbine inlet temperature (receiver outlet temperature) of ≈ 875 °C, which is the optimum receiver operating temperature for a concentration ratio $C = 500$ (see Fig. 6), the combined cycle thermal-to-electric efficiency (Fig. 8) almost reaches 47%. In order to achieve a breakthrough in thermal-to-electric conversion efficiencies, say 50% and better, the receiver must operate at outlet temperatures above 1000 °C, which would require mean concentration ratios C larger than 1000, values which are very difficult to reach in practice (practical concentration limit).

5.1.1. Solar combined cycle with reheated BC vs. non-reheated BC

Next, the performance of the solar combined cycle with reheated BC will be compared to that without reheat in the topping cycle (see Fig. 5).

The important difference compared to the reheated version is that there is no parameter available to modify the BC exit temperature apart from the pressure ratio (\approx expansion ratio). Hence, the TET is fixed for a given TIT and pressure ratio.

As shown in Table 5, the performance of the solar combined cycle, without reheat in the topping cycle, is considerably lower (24.4% vs. 27.1% when $C = 500$ - see Table 4). Also the optimum pressure ratio (≈ 3) is lower than in the case of the reheated BC,

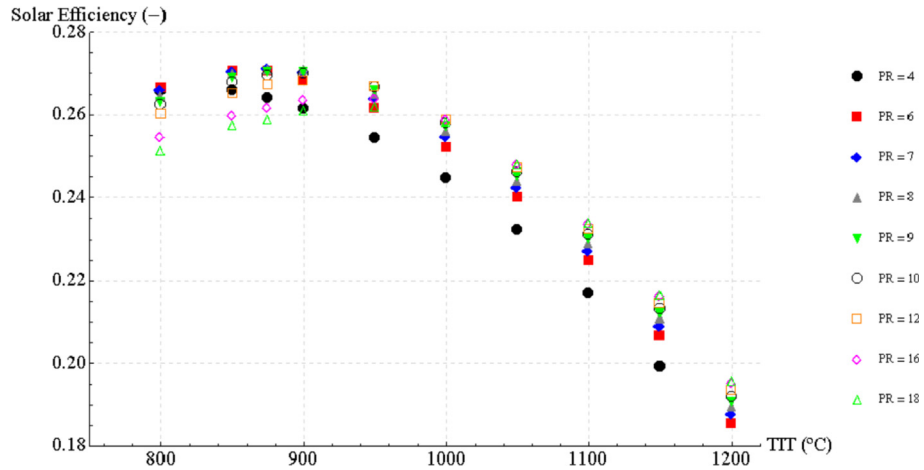


Fig. 6. Solar combined cycle solar-to-electric performance as function of BC TIT and BC pressure ratio for $C = 500$ and $K = 1.25$.

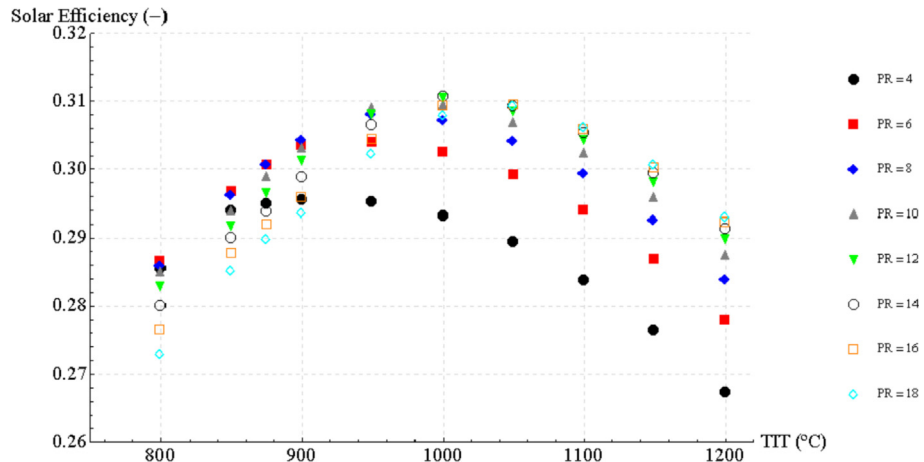


Fig. 7. Solar combined cycle solar-to-electric performance as function of BC TIT and BC pressure ratio for $C = 1000$ and $K = 1$.

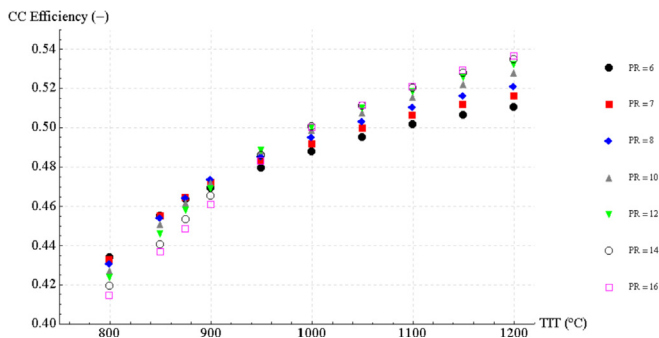


Fig. 8. Combined cycle thermal-to-electric efficiency vs. gas turbine inlet temperature and pressure ratio for $K = 1.25$.

which however is an advantage as the useable ΔT for the TES increases (lower compressor outlet temperature).

Fig. 9 and Fig. 10 display the solar-to-electric performance as function of TIT and pressure ratio for concentration ratio $C = 500$ and $C = 1000$, respectively.

Table 5

Optimum values of non-reheated BC TIT (receiver outlet temperature) and PR.

C (-)	optimum TIT (°C)	optimum PR (-)	$\eta_{solar-to-electric}$ (%)
500	900	3	24.4%
1000	1050	5	28.6%

5.1.2. Benchmarking of the solar combined cycle against solar single cycle power plant options

The single cycle plant options are (i) the parabolic trough collector plant using thermal oil as HTF (maximum HTF temperature of 391 °C, and Rankine live steam conditions of 371 °C, 100 bar), (ii) the molten salt power tower plant (maximum HTF temperature of 565 °C, and Rankine live steam conditions of 545 °C, 125 bar) in single and multi-tower configuration, (iii) the open volumetric air receiver power tower plant according to Fig. 11, however in multi-tower configuration, and finally (iv) a power tower plant driving a reheated Brayton cycle only, also in multi-tower configuration. The latter configuration is added to see the performance of a solar powered reheated BC, optimized for the single-cycle operation (note that in combined cycle configuration, the BC does not run in its optimum point due to the TET constraint). Table 6 summarizes the performance comparison. The annual plant conversion

Table 6
Solar thermal power plant performance parameters for benchmarking (related to Fig. 12).

Plant configuration (Label in Fig. 12)	Solar field optical peak efficiency (-)	Receiver efficiency (-)	Power block thermal-to-electric net* efficiency (-) at 25 °C ambient temperature	Maximum HTF temperature (°C)	Solar-to-electric peak conversion efficiency (-)	Solar-to-electric annual mean conversion efficiency (-)
Oil parabolic trough plant (Oil Trough SC) [41–44]	0.77	0.78	0.3 (dry air cooled Rankine)	391	0.18	0.143
Molten salt single-tower plant - 933,724 m ² aperture area surround field (MS S-Tower SC)	0.66 [45]	0.85 (Eq. (7))	0.38 (dry air cooled Rankine)	565	0.213	0.155
Molten salt multi-tower plant - 80,216 m ² aperture area north fields (MS M-Tower SC)	0.8 [26]	0.85 (Eq. (7))	0.365 (dry air cooled Rankine)	565	0.248	0.19
Open volumetric air central receiver multi-tower plant with Rankine steam cycle (Air R SC)	0.8 [26]	0.81 (Eq. (7))	0.358 (According to Table 3)	–	0.232 (C = 500, Fig. 12)	0.175 (C = 500, Receiver temperature = 700 °C)
Multi-tower central receiver plant powering a reheated Brayton cycle (BC SC)	0.8 [26]	0.683 (Eq. (7))	0.299 (According to Section 4.1)	–	0.163 (C = 500, Fig. 12)	0.10 (C = 500, Receiver temperature = 950 °C)
Multi-tower central receiver plant powering a combined cycle with single reheat in BC (CC)	0.8 [26]	0.729 (Eq. (7))	0.465 (According to Section 5.1)	–	0.271 (C = 500, Fig. 12)	0.21 (C = 500, Receiver temperature = 875 °C)

* the power block net efficiency includes the parasitic power consumption of HTF pumping (the multi-tower approach increases HTF pumping)

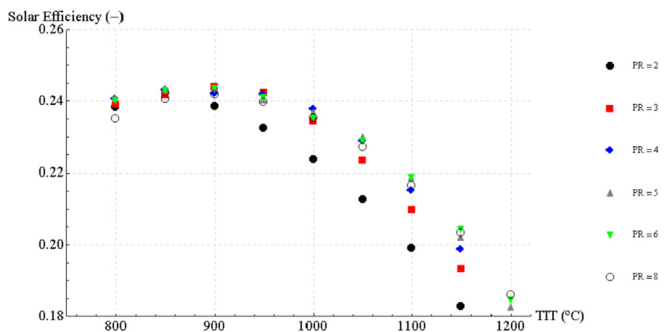


Fig. 9. Solar combined cycle solar-to-electric performance as function of BC TTT and pressure ratio for C = 500 (non-reheated BC).

efficiency values have been obtained running annual energy yield simulations using a typical meteorological year for Seville, Spain.

Fig. 12 displays the benchmarking results. For a moderate mean concentration ratio of C = 500, the optimized solar combined cycle performance (27.1%) is just 2.3 percentage points above the molten salt multi-tower configuration (24.8%) and added plant complexity

and elevated operating temperatures (≈ 875 °C) of the combined cycle option will very likely result in effectively more expensive electricity production.

For a mean concentration ratio C = 1000 (\approx practical concentration limit), the optimized solar combined cycle performance (31.1%) is well above current state-of-the-art technology. Nevertheless, also here a techno-economic evaluation is required to justify the added plant complexity.

The performance of the single-cycle reheated BC plant stays well below the performance of conventional molten salt and trough technology for moderate mean concentration ratios (C = 500), and also at higher concentration ratios no significant performance improvement can be achieved.

Last but not least, the multi-tower open volumetric air receiver technology with single-cycle Rankine (Air R SC, Fig. 12) seems to be a very interesting alternative to conventional molten salt towers, as air as heat transfer fluid has several advantages regarding plant operation (no freezing, robust receiver technology) and also regarding investment (cheap TES, no HTF costs). Nevertheless, pressure drop and thus parasitic power consumption of the atmospheric air circuit is an issue that needs to be considered during plant design (air flow velocities must be kept low). A typical value

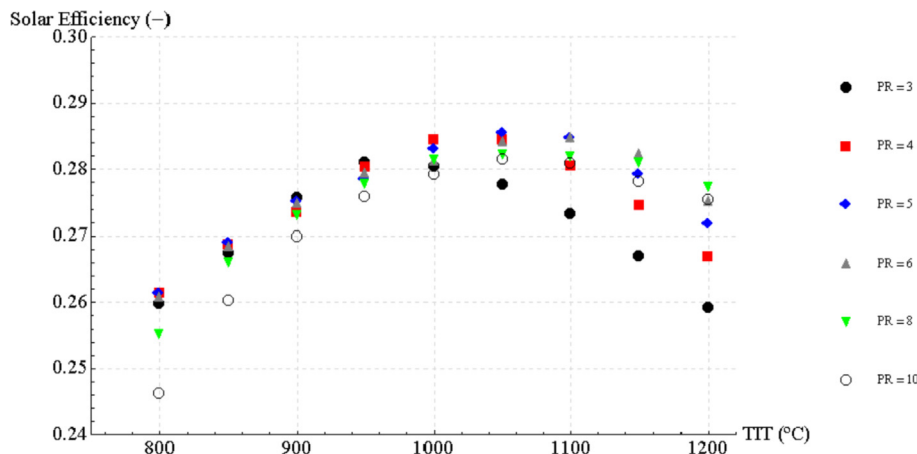


Fig. 10. Solar combined cycle solar-to-electric performance as function of BC TTT and pressure ratio for C = 1000 (non-reheated BC).

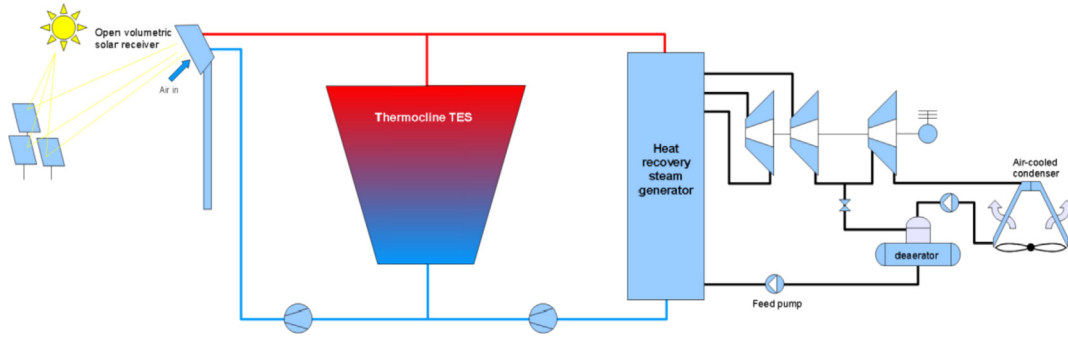


Fig. 11. Single cycle Rankine scheme – Plant concept according to Refs. [39,40].

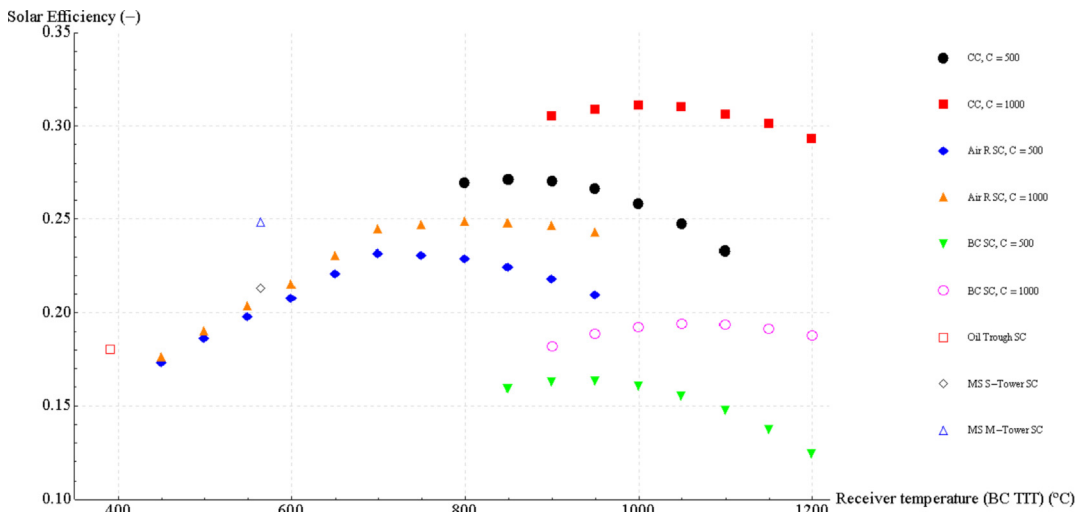


Fig. 12. Solar-to-electric peak efficiency as function of receiver temperature (BC TIT), concentration ratio C and plant configuration (CC: solar combined cycle, Air R SC: Rankine single cycle with air receiver, BC SC: Brayton single cycle, Oil Trough SC: Parabolic trough plant with Rankine single cycle, MS S-Tower SC: Molten salt single tower with Rankine single cycle, MS M-Tower SC: Molten salt multi tower with Rankine single cycle).

for the total air loop pressure drop (solar receiver, air ducts, heat recovery steam generator) is in the range of 4–5 kPa (a pressure drop of 5 kPa has been used in this study).

5.2. Performance of the solar combined cycle with volumetric receiver behavior

Again, the compressor pressure ratio and the reheat ratio K has been optimized for each value of concentration ratio C (500, 1000). As the optimum receiver outlet temperature moves to higher values, also the optimum value of K reduces, compared to non-volumetric receiver behavior. In particular, for concentration ratio $C = 500$, K optimizes at about 0.75, whereas for concentration ratio $C = 1000$, K optimizes at about 0.5 (see Table 7). Fig. 13 and Fig. 14 display the solar-to-electric conversion efficiency as function of TIT and gas turbine pressure ratio for concentration ratio $C = 500$ and $C = 1000$, respectively.

In summary, the open volumetric air receiver technology can significantly boost the solar combined cycle performance. For realistic power tower mean concentration ratios ($C \approx 500$), the optimum conversion efficiency is obtained at a turbine inlet temperature (receiver outlet temperature) of about 1050 °C, and a pressure ratio of 14 (Fig. 13), which seem to be realistic design targets. Furthermore, by reaching TITs of 1050 °C, the thermal-to-electric combined cycle conversion efficiency may touch the 50%

Table 7
Optimum values of reheated BC TIT (receiver outlet temperature) and PR for given values of K – volumetric receiver behavior.

C (-)	K (-)	optimum TIT (°C)	optimum PR (-)	$\eta_{solar-to-electric}$ (%)
500	0.75	1050	14	29.6%
1000	0.5	1250	24	33.1%

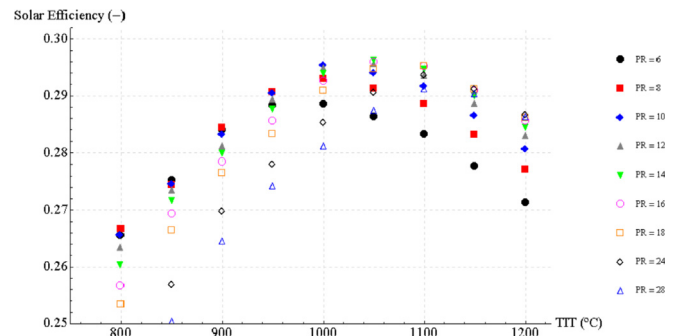


Fig. 13. Volumetric receiver solar combined cycle solar-to-electric performance as function of BC TIT and BC pressure ratio for $C = 500$ and $K = 0.75$.

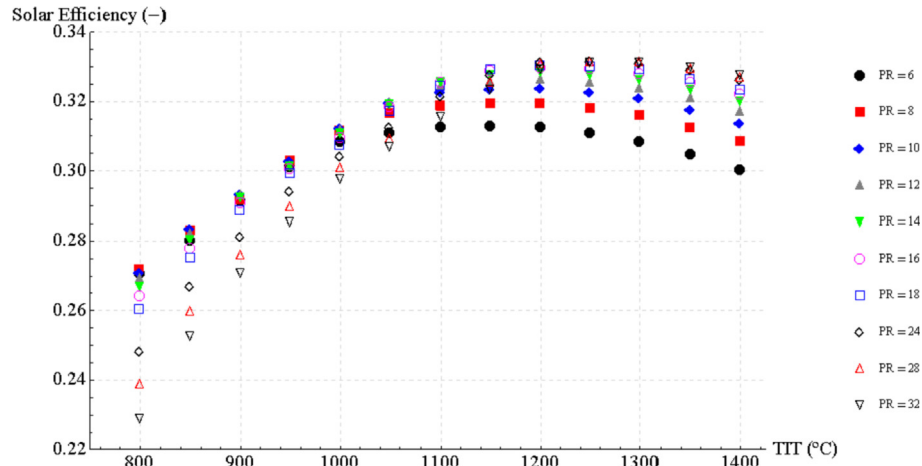


Fig. 14. Volumetric receiver solar combined cycle solar-to-electric performance as function of BC TIT and BC pressure ratio for $C = 1000$ and $K = 0.5$.

threshold (see Fig. 15), meaning a significant power cycle improvement with respect to current state-of-the-art CSP technology. However, for higher concentration ratios, the optimum receiver outlet temperatures (TITs) exceed 1200 °C, which is very likely too high for competitive air-air heat exchanger technology due to material limitations and elevated costs. Additionally, very high optimum compressor pressure ratios limit the integration with thermal energy storage (lower ΔT for TES). Furthermore, as the performed simulations consider an uncooled gas turbine, the results for very high TITs (≥ 1100 °C) are of theoretical nature only.

5.2.1. Solar combined cycle with reheated BC vs. non-reheated BC

Also for the case of a solar combined cycle, powered by a volumetric receiver, the simple non-reheated BC configuration has been analyzed (Table 8). In this case, reheat may increase overall plant performance by up to about 2 percentage points, which is lower than in the case of non-volumetric receiver behavior.

5.2.2. Benchmarking of the volumetric receiver solar combined cycle against solar single cycle power plant options

Due to the volumetric effect (higher receiver efficiency at elevated operating temperatures), the solar combined cycle already exceeds at a moderate concentration ratio ($C = 500$) the performance of conventional CSP technology (oil trough, molten salt

Table 8

Optimum values of non-reheated BC TIT (receiver outlet temperature) and PR – volumetric receiver behavior.

C (-)	optimum TIT (°C)	optimum PR (-)	$\eta_{solar-to-electric}$ (%)
500	1100	5	27.6%
1000	1300	10	31.5%

single- and multi tower) significantly (Fig. 16).

Again, the multi-tower open volumetric air receiver technology (Fig. 16 “Air R SC”) with single-cycle Rankine seems to be a very interesting alternative to conventional molten salt towers.

Last but not least, the performance of the single-cycle reheated BC plant (Fig. 16 BC SC) catches up with parabolic trough technology for moderate concentration ratios ($C = 500$) and viable turbine inlet temperatures of just above 1000 °C. However, also at higher concentration ratios no performance improvement can be achieved with respect to molten salt central receiver technology.

6. Conclusions

This work discusses the performance of solar powered combined cycles, comparing the performance of opaque-heat-exchanger-type receivers with that of open volumetric air

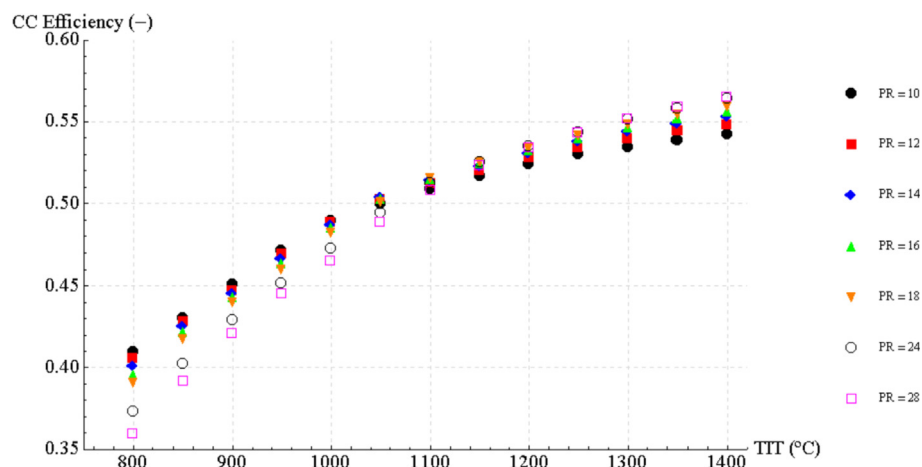


Fig. 15. Combined cycle thermal-to-electric efficiency vs. gas turbine inlet temperature and pressure ratio – $K = 0.75$.

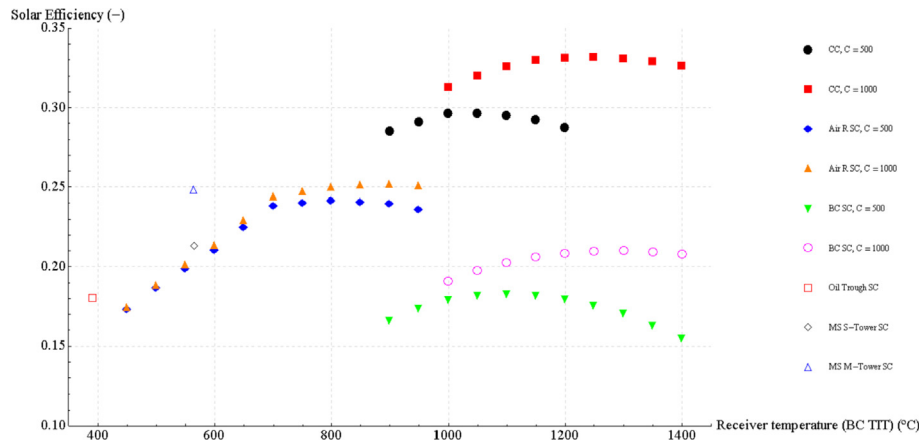


Fig. 16. Solar-to-electric peak efficiency as function of receiver temperature (BC TIT), concentration ratio C and plant configuration (CC: solar combined cycle, Air R SC: Rankine single cycle with air receiver, BC SC: Brayton single cycle, Oil Trough SC: Parabolic trough plant with Rankine single cycle, MS S-Tower SC: Molten salt single tower with Rankine single cycle, MS M-Tower SC: Molten salt multi tower with Rankine single cycle).

receivers. It is shown that open volumetric air receivers can significantly boost solar combined cycle performance (up to 3.2 percentage points, depending on concentration ratio C and BC configuration) due to the so-called volumetric effect, which improves solar receiver efficiency at high operating temperatures, which in turn are crucial for good thermal-to-electric conversion efficiencies. However, the proposed plant concept requires an additional heat exchanger for the heat exchange between atmospheric air (i.e. the heat transfer fluid) and pressurized air (i.e. the working fluid of the power cycle), which is not an easy design task. One possibility is a regenerative air-air heat exchanger (atmospheric heating and pressurized cooling). Nevertheless, the pressure drop of the atmospheric air loop is critical and must be kept low.

Furthermore, it is shown that a solar combined cycle with reheated topping cycle behaves significantly better than its non-reheated counterpart. The performance difference is up to about 2.7 percentage points.

At a moderate concentration ratio of $C = 500$, the solar-to-electric performance of a solar combined cycle, powered by an opaque-heat-exchanger-type (non-volumetric) receiver and applying a non-reheated Brayton cycle, is below that of the molten salt multi-tower configuration (24.4% vs. 24.8%). Thus, added plant complexity and elevated operating temperatures (≈ 900 °C) of the combined cycle option will result in more expensive electricity production. Clearly, future work will have to deal with the techno-economic optimization and comparison of competing CSP technology.

An important conclusion is that the optimum solar combined cycle performance for moderate mean concentration ratios ($C \approx 500$) is fully compatible with available high-temperature TES (packed-bed thermocline), providing the promising possibility of dispatchable operation at highest thermal-to-electric conversion efficiency. However, in order to boost the solar-to-electric plant performance significantly above that of molten salt central receivers, the solar receiver must work at sufficiently high efficiencies. The open volumetric air receiver is a very promising solution. According to the results of this work, 29.6% of peak solar-to-electric conversion efficiency can be achieved already for a moderate mean concentration ratio $C = 500$, which is a significant improvement with respect to state-of-the-art technology. Nevertheless, it is clear that compact power plant layouts (<330 MW total nominal solar power) are the preferred choice for the presented

power plant concept that applies atmospheric air as HTF, as large diameter piping (low air speeds are mandatory) becomes an issue at higher power classes, not only in terms of investment, but also in terms of thermal inertia and thermal losses. Forthcoming work of the authors will have to deal with the detailed techno-economic evaluation, which has to show whether the thermodynamic advantage of the proposed plant concept also pays off from the economic point of view.

Acknowledgements



This work has received funding from the European Union's Horizon 2020 research and innovation program under the grant agreement No 640905.

The authors gratefully acknowledge the work of the six anonymous reviewers, whose comments and suggestions significantly improved the quality of the paper.

Appendix

Derivation of Eq. (7):

Using the effective solar flux concentration ratio C_{flux} , the mean solar flux density I (W/m^2) incident on the receiver is therefore:

$$I = C_{flux} \cdot DNI \quad (7a)$$

The receiver's thermal behavior can be very well summarized by the following simple equations, stating a basic steady-state energy

balance.

The useful thermal power P_{HTF} that can be delivered to the heat transfer fluid (HTF) is equal to the absorbed solar power (incident solar power P_s multiplied by the solar absorptance α), reduced by the thermal losses P_{loss} due to radiation and convection:

$$P_{HTF} = P_s \cdot \alpha - P_{loss} \quad (7b)$$

with

$$P_s = I \cdot A_r = C_{flux} \cdot DNI \cdot A_r \quad (7c)$$

and

$$P_{loss} = P_{rad} + P_{con} = A_r \cdot [\varepsilon \cdot \sigma \cdot (T_r^4 - T_a^4) + h \cdot (T_r - T_a)] \quad (7d)$$

The solar receiver's efficiency η_r can then be defined as the ratio of useful thermal power delivered to the heat transfer fluid P_{HTF} to total incident solar power P_s :

$$\eta_r = \frac{P_{HTF}}{P_s} = \frac{P_s \cdot \alpha - P_{loss}}{P_s} = \alpha - \frac{P_{loss}}{P_s} \quad (7e)$$

Thus, inserting the complete terms for P_{loss} and P_s from above, the following equation for the receiver's efficiency is obtained (note that A_r cancels out):

$$\eta_r = \alpha - \frac{\varepsilon \cdot \sigma \cdot (T_r^4 - T_a^4) + h \cdot (T_r - T_a)}{C_{flux} \cdot DNI} \quad (7)$$

Derivation of Eq. (8):

The solar-to-thermal efficiency of a central receiver plant is the ratio of useful thermal power delivered to the heat transfer fluid (P_{HTF}), to the total power theoretically available for the plant (P_{SF}). The total power theoretically available (P_{SF}) is defined by the product of total aperture area (heliostat area times number of heliostats) and direct normal irradiance (DNI).

$$\eta_{solar-to-thermal} = \frac{P_{HTF}}{P_{SF}} \quad (8a)$$

$$P_{HTF} = P_s \cdot \alpha - P_{loss} \quad (8b)$$

$$P_{SF} = A_a \cdot DNI \quad (8c)$$

As described above, the useful power delivered to the heat transfer fluid is the absorbed solar power (incident solar power P_s times solar absorptivity) at the receiver reduced by the thermal losses (Eq. (8b)). In this case, the incident solar power at the receiver P_s is calculated as follows:

$$P_s = A_a \cdot DNI \cdot \eta_f \quad (8d)$$

Substituting P_{HTF} and P_{SF} in Eq. (8a) for the correlations given in Eq. (8b) to Eq. (8d) yields the following relationship for the efficiency of the solar-to-thermal energy conversion process:

$$\eta_{solar-to-thermal} = \frac{A_a \cdot DNI \cdot \eta_f \cdot \alpha - A_r \cdot [\varepsilon \cdot \sigma \cdot (T_r^4 - T_a^4) + h \cdot (T_r - T_a)]}{A_a \cdot DNI} \quad (8e)$$

Next, DNI and A_a cancel out in the first part of the equation, simplifying the correlation as follows:

$$\eta_{solar-to-thermal} = \eta_f \cdot \alpha - \frac{\varepsilon \cdot \sigma \cdot (T_r^4 - T_a^4) + h \cdot (T_r - T_a)}{C_{hyp} \cdot DNI} \quad (8f)$$

When substituting the hypothetical concentration ratio C_{hyp} for $\frac{C_{flux}}{\eta_r}$ (see Eq. (6)), the following equation is obtained:

$$\eta_{solar-to-thermal} = \eta_f \cdot \alpha - \frac{\varepsilon \cdot \sigma \cdot (T_r^4 - T_a^4) + h \cdot (T_r - T_a)}{\frac{C_{flux}}{\eta_r} \cdot DNI} \quad (8g)$$

Now, the equation can be simplified, factoring η_f out, to yield Eq. (8).

$$\eta_{solar-to-thermal} = \eta_f \cdot \alpha - \frac{\eta_f \cdot [\varepsilon \cdot \sigma \cdot (T_r^4 - T_a^4) + h \cdot (T_r - T_a)]}{C_{flux} \cdot DNI} \quad (8h)$$

$$\eta_{solar-to-thermal} = \eta_f \cdot \left[\alpha - \frac{\varepsilon \cdot \sigma \cdot (T_r^4 - T_a^4) + h \cdot (T_r - T_a)}{C_{flux} \cdot DNI} \right] \quad (8i)$$

$$\eta_{solar-to-thermal} = \eta_f \cdot \eta_r \quad (8)$$

References

- [1] Ho CK. Advances in central receivers for concentrating solar applications. Sol Energy 2017;152:38–56.
- [2] Ibrahim Tk, Mohammed MK, Awad OI, Rahman MM, Najafi G, Basrawi F, Abd Alla AN, Mamat R. The optimum performance of the combined cycle power plant: a comprehensive review. Renew Sustain Energy Rev 2017;79:459–74.
- [3] Miller J. The combined cycle and variations that use HRSGs. In: Eriksen VL, editor. Heat recovery steam generator technology. Duxford, United Kingdom: Woodhead Publishing; 2017. p. 17–43.
- [4] Al-attab KA, Zainal ZA. Externally fired gas turbine technology: a review. Appl Energy 2015;138:474–87.
- [5] Becker B, Finckh HH, Meyer-Pittroff R. Combined gas and steam cycle for a gas-cooled solar tower power plant. J. Eng. Power 1982;104:330–40.
- [6] Fraidenaich N, Gordon JM, Tiba C. Optimization of gas-turbine combined cycles for solar energy and alternative-fuel power generation. Sol Energy 1992;48:301–7.
- [7] Kribus A, Zaibel R, Carey D, Segal A, Karni J. A solar-driven combined cycle power plant. Sol Energy 1998;62:121–9.
- [8] Karni J, Rubin R, Sagie D, Fiterman A, Kribus A, Doron P. The DIAPR: a high-pressure, high-temperature solar receiver. J Sol Energy Eng 1997;119:74–8.
- [9] Puppe M, Giuliano S, Krüger M, Lammel O, Buck R, Boje S, Saidi K, Gampe U, Felsmann C, Freimark M, Langnickel U. Hybrid high solar share gas turbine systems with innovative gas turbine cycles. Energy Procedia 2015;69:1393–403.
- [10] Grange B, Dalet C, Falcoz Q, Ferrière A, Flamant G. Impact of thermal energy storage integration on the performance of a hybrid solar gas-turbine power plant. Appl Therm Eng 2016;105:266–75.
- [11] Pozivil P, Steinfeld A. Integration of a pressurized-air solar receiver array to a gas turbine power cycle for solar tower applications. J Sol Energy Eng 2017;139. 041007-041007-041008.
- [12] Siros F, Fernández Campos G. Optimisation of a low-TIT combined cycle gas turbine with application to new generation solar thermal power plants. ASME. Charlotte, NC, USA: ASME Turbo Expo 2017; 2017. V003T006A038.
- [13] Becker M. Gast - the gas cooled solar tower technology program. Berlin Heidelberg, Germany: Springer Verlag; 1989.
- [14] Ávila-Marín AL. Volumetric receivers in solar thermal power plants with central receiver system technology: a review. Sol Energy 2011;85:891–910.
- [15] Korzynietz R, Brioso JA, del Río A, Quero M, Gallas M, Uhlig R, Ebert M, Buck R, Teraji D. Solugas – comprehensive analysis of the solar hybrid Brayton plant. Sol Energy 2016;135:578–89.
- [16] Hennecke K, Schwarzbözl P, Alexopoulos S, Göttsche J, Hoffschmidt B, Beuter M, Koll G, Hartz T. Solar power tower Jülich - the first test and demonstration plant for open volumetric receiver technology in Germany. USA: SolarPACES, Las Vegas; 2008.
- [17] CENER. Horizon 2020 research project "CAPture - competitive SolAr power towers" - grant agreement number 640905. 2015. www.capture-solar-energy.eu/.
- [18] Kwakernaak H, Tijssen P, Stribos RCW. Optimal operation of blast furnace

- stoves. *Automatica* 1970;6:33–40.
- [19] Zanganeh G, Pedretti A, Zavattoni S, Barbato M, Steinfeld A. Packed-bed thermal storage for concentrated solar power – pilot-scale demonstration and industrial-scale design. *Sol Energy* 2012;86:3084–98.
- [20] ALACAES-SA. ALACAES - creating sustainable energy solutions for a brighter future. Switzerland: Lugano; 2017. <https://alacaes.com/>.
- [21] Polyzakis AL, Koroneos C, Xydís G. Optimum gas turbine cycle for combined cycle power plant. *Energy Convers Manag* 2008;49:551–63.
- [22] Sheikhbeigi B, Ghofrani MB. Thermodynamic and environmental consideration of advanced gas turbine cycles with reheat and recuperator. *Int J Environ Sci Technol* 2007;4:253–62.
- [23] Romero M, Buck R, Pacheco JE. An update on solar central receiver systems, projects, and technologies. *J Sol Energy Eng* 2002;124:98–108.
- [24] Romero-Alvarez M, Zarza E, Kreith F, Goswami DY. Handbook of energy efficiency and renewable energy. Boca Raton, USA: CRC Press Taylor and Francis Group; 2007.
- [25] McGovern RK, Smith WJ. Optimal concentration and temperatures of solar thermal power plants. *Energy Convers Manag* 2012;60:226–32.
- [26] Mutuberría A, Les I, Schöttl P, Leonardi E, Bonanos A. Report on heliostat field layout design - STAGE-STE Project Deliverable 12.7 - FP7. 2017. Grant Agreement number: 609837.
- [27] Hoffschmidt B, Téllez FM, Valverde A, Fernández J, Fernández V. Performance evaluation of the 200-kWth HiTRec-II open volumetric air receiver. *J Sol Energy Eng* 2003;125:87–94.
- [28] Heller P, Pfänder M, Denk T, Tellez F, Valverde A, Fernandez J, Ring A. Test and evaluation of a solar powered gas turbine system. *Sol Energy* 2006;80:1225–30.
- [29] Pozivil P, Ackermann S, Steinfeld A. Numerical heat transfer analysis of a 50 kWth pressurized-air solar receiver. *J Sol Energy Eng* 2015;137. 064504-064504-064504.
- [30] Zaversky F, Aldaz L, Sánchez M, Ávila-Marín AL, Roldán MI, Fernández-Reche J, Füssel A, Beckert W, Adler J. Numerical and experimental evaluation and optimization of ceramic foam as solar absorber – single-layer vs multi-layer configurations. *Appl Energy* 2018;210:351–75.
- [31] Zaversky F, Aldaz L, Sánchez M, Avila-Marín AL, Roldán MI, Fernández-Reche J, Füssel A, Beckert W, Adler J. Ceramic foam absorber modeling and optimization - model benchmarking and validation against experimental data. Abu Dhabi: SolarPACES; 2016. UAE.
- [32] Pabst C, Feckler G, Schmitz S, Smirnova O, Capuano R, Hirth P, Fend T. Experimental performance of an advanced metal volumetric air receiver for Solar Towers. *Renew Energy* 2017;106:91–8.
- [33] Wagner W, Kruse A. Properties of water and steam: the industrial standard IAPWS-IF97 for the thermodynamic properties and supplementary equations for other properties: tables based on these equations. Springer-Verlag; 1998.
- [34] Thermoflow-Inc. GT PRO - gas turbine combined cycle design program to create cycle heat balance and physical equipment needed to realize it. 2018. http://www.thermoflow.com/combinedcycle_GTP.html. [Accessed 27 July 2018].
- [35] McBride BJ, Zehe MJ, Gordon S. NASA glenn coefficients for calculating thermodynamic properties of individual species. Cleveland, Ohio, USA: Glenn Research Center; 2002.
- [36] Jackson BN. 4 - vertical tube natural circulation evaporators. In: Eriksen VL, editor. Heat recovery steam generator technology. Woodhead Publishing; 2017. p. 65–80.
- [37] Elmqvist H, Mattsson SE. Modelica - the next generation modeling language - an international design effort. In: Proceedings of the 1st world congress on system simulation; 1997. Singapore.
- [38] Ganapathy V. Industrial boilers and heat recovery steam generators - design, applications, and calculations. New York, USA: Marcel Dekker, Inc., 270 Madison Avenue; 2003.
- [39] Fricker HW. Regenerative thermal storage in atmospheric air system solar power plants. *Energy* 2004;29:871–81.
- [40] Hennecke K, Hoffschmidt B, Koll G, Schwarzbözl P, Götsche J, Beuter M, Hartz T. The solar power tower Jülich - a solar thermal power plant for test and demonstration of air receiver technology. Beijing, China: ISES World Congress; 2007.
- [41] Romero M, González-Aguilar J. Solar thermal CSP technology3. Wiley Interdisciplinary Reviews: Energy and Environment; 2014. p. 42–59.
- [42] Zaversky F, Bergmann S, Sanz W. Detailed modeling of parabolic trough collectors for the part load simulation of solar thermal power plants - GT2012-68032. Copenhagen, Denmark: Proceedings of the ASME Turbo Expo; 2012. p. 235–47.
- [43] Price H. Assessment of parabolic trough and power tower solar technology cost and performance forecasts. Golden, Colorado, USA: NREL - National Renewable Energy Laboratory; 2003.
- [44] Zhang HL, Baeyens J, Degrève J, Caçeres G. Concentrated solar power plants: review and design methodology. *Renew Sustain Energy Rev* 2013;22:466–81.
- [45] Avila-Marín AL, Fernandez-Reche J, Tellez FM. Evaluation of the potential of central receiver solar power plants: configuration, optimization and trends. *Appl Energy* 2013;112:274–88.